Physics Letters B 695 (2011) 124–129

Contents lists available at ScienceDirect

Physics Letters B

www.elsevier.com/locate/physletb

First dark matter search results from a surface run of the 10-L DMTPC directional dark matter detector

DMTPC Collaboration

S. Ahlen [d], J.B.R. Battat [f], T. Caldwell [f], C. Deaconu [f], D. Dujmic [a,f], W. Fedus [f], P. Fisher [a,b,f], F. Golub [e], S. Henderson [f], A. Inglis [d], A. Kaboth [f], G. Kohse [c], R. Lanza [c], A. Lee [f], J. Lopez [f], J. Monroe [f,*], T. Sahin [f], G. Sciolla [f], N. Skvorodnev [e], H. Tomita [d], H. Wellenstein [e], I. Wolfe [f], R. Yamamoto [f], H. Yegoryan [f]

[a] *Laboratory for Nuclear Science, Massachusetts Institute of Technology, Cambridge, MA 02139, United States*
[b] *MIT Kavli Institute for Astrophysics and Space Research, Massachusetts Institute of Technology, Cambridge, MA 02139, United States*
[c] *Nuclear Science and Engineering Department, Massachusetts Institute of Technology, Cambridge, MA 02139, United States*
[d] *Physics Department, Boston University, Boston, MA 02215, United States*
[e] *Physics Department, Brandeis University, Waltham, MA 02453, United States*
[f] *Physics Department, Massachusetts Institute of Technology, Cambridge, MA 02139, United States*

ARTICLE INFO

Article history:
Received 2 September 2010
Received in revised form 19 November 2010
Accepted 21 November 2010
Available online 25 November 2010
Editor: S. Dodelson

Keywords:
Dark matter
WIMP
Direction-sensitive
Time projection chamber

ABSTRACT

The Dark Matter Time Projection Chamber (DMTPC) is a low pressure (75 Torr CF_4) 10 liter detector capable of measuring the vector direction of nuclear recoils with the goal of directional dark matter detection. In this Letter we present the first dark matter limit from DMTPC from a surface run at MIT. In an analysis window of 80–200 keV recoil energy, based on a 35.7 g-day exposure, we set a 90% C.L. upper limit on the spin-dependent WIMP-proton cross section of 2.0×10^{-33} cm^2 for 115 GeV/c^2 dark matter particle mass.

1. Introduction

Despite strong astrophysical evidence that dark matter comprises approximately 23% of our universe [1], the nature of this dark matter remains largely unknown. Weakly interacting massive particles (WIMPs) are a favored dark matter candidate [2]. Many indirect and direct detection experiments aim to discover and measure the properties of WIMPs [3]. Direct WIMP detection experiments search for the interaction of WIMPs with a nucleus in the detector, resulting in low-energy nuclear recoils [4]. Most experiments seek to detect the kinetic energy deposited by the recoiling nucleus; a handful of recent efforts, including this work, also seek to detect the direction of the nuclear recoil, and in this way, infer the direction of incoming WIMPs [5–11]. The arrival direction of WIMPs is predicted to peak in the direction opposite to the earth's motion around the galactic center in the simplest dark matter halo model, and have a time-varying asymmetry because the Earth's rotation gives angular modulation in time [12]. The angular signature of directional detection offers the potential for unambiguous observation of dark matter [13]. This Letter presents the first dark matter limit from the DMTPC directional detection experiment, from a surface run at MIT.

2. The dark matter time projection chamber experiment

DMTPC is a dark matter detector designed to measure the direction and energy of recoiling fluorine nuclei. CF_4 is chosen as a target due to good scintillation characteristics [14] and the relatively large predicted axial-vector coupling for fluorine, allowing sensitivity to spin-dependent WIMP interactions [15,16].

The detector consists of two optically isolated back-to-back low-pressure time projection chambers, with a $14.6 \times 14.6 \times 19.7$ cm^3 ($15.9 \times 15.9 \times 19.7$ cm^3) fiducial volume for the top (bottom) TPC. The TPCs are filled with 75 ± 0.1 Torr of CF_4 corresponding to a

* Corresponding author.
E-mail address: jmonroe@mit.edu (J. Monroe).

0370-2693
doi:10.1016/j.physletb.2010.11.041

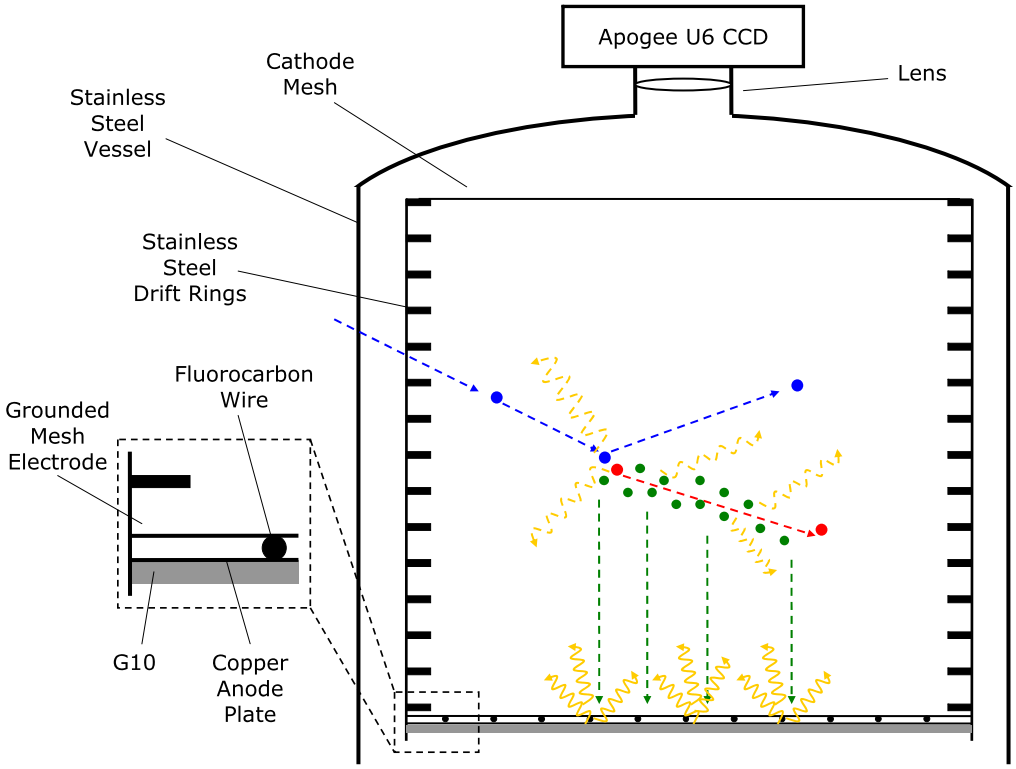

Fig. 1. A schematic of one TPC (not to scale). A WIMP (blue) induces a nuclear recoil (red) which produces ionization electrons (green) and scintillation light (yellow).

3.3 g (2.85 g) fiducial mass of CF_4 (F). In 75 Torr of CF_4, a recoiling fluorine nucleus with 50 keV kinetic energy would travel approximately 1 mm before stopping. The cathode and ground planes of the TPC are 27 cm diameter meshes with 256 μm pitch. The grounded mesh sits 0.5 mm from the copper-clad G10 anode plate (see Fig. 1). Ionization electrons from interactions in the fiducial volume drift in a uniform electric field of 0.25 kV/cm towards the amplification region (14.4 kV/cm) where avalanche multiplication amplifies the electron signal and produces scintillation. The wavelength spectrum of the scintillation light peaks at ~ 600 nm, with roughly two-thirds of the scintillation emission in the visible [14]. The gas gain is approximately 4×10^4, measured with an ^{55}Fe calibration source. The operating anode voltage is chosen to maximize the gain while limiting the rate of electronic discharge between the anode and ground plane to < 0.025 Hz. The drift electric field is chosen to minimize the transverse diffusion of the drifting electrons. For a more detailed discussion of the 10 liter detector amplification and diffusion, see [17] and [18].

Scintillation light produced in the amplification region is focussed by a Nikon photographic lens (f/1.2, 55 mm focal length) onto an Apogee Alta U6 camera containing a 1024×1024 element Kodak 1001E CCD chip with 24×24 μm^2 pixels. The CCD clock rate is 1 MHz with 16-bit digitization, and typical readout time is 0.2 s. With this camera we are read-noise limited. To improve the signal-to-noise ratio (and to reduce deadtime from CCD readout), pixels are binned 4×4 prior to digitization. In addition to optical readout, we also digitize the integrated charge induced on the anode, although we do not use the charge data in this analysis.

The surface run data set consists of 231,000 five-second CCD exposures from each camera, collected without trigger or camera shutter. Of these, 10.5% and 4.4% are rejected by analysis cuts as spark events in the top and bottom TPCs respectively, and 3.5×10^{-3}% and 8.7×10^{-4}% as the associated residual bulk image (RBI) background pixels (described in Section 2.2) respectively. After correcting the live time for these analysis cuts, the data set live time averaged over the two cameras is 12.35 days. This does not include parasitic exposure (when pixels are exposed during CCD readout and event writing), which increases the live time by approximately 11%. The data taking efficiency was approximately 65%, including time for gas refilling.

2.1. Calibration and reconstruction

Track length and energy calibrations employ ^{241}Am alpha sources at fixed locations in the top and bottom TPCs. The calibration sources are placed inside each TPC, on the field cage rings. The energies of the two sources, used for top and bottom TPC calibrations, are 4.51 ± 0.05 MeV and 4.44 ± 0.05 MeV respectively. These energies come from independent measurements of each source with a Canberra 450-20AM surface barrier detector, calibrated with decay alphas from radon-enriched N_2 gas. The energies are slightly different for the two sources, likely because of differences in thickness of the thin gold windows of each of the source holders. The length calibration relies on the known horizontal separation, 2.5 ± 0.1 cm, of resistive separators in the amplification region, shown in Fig. 1. Tracks from alphas have decreased light yield at the spacer locations. Fitting Gaussian profiles to these regions gives the spacer positions in the image plane, and shows that each 24 μm × 24 μm CCD pixel images 143 ± 3 μm × 143 ± 3 μm (156 ± 3 μm × 156 ± 3 μm) of the top (bottom) anode.

The energy response of the detector is obtained from the same data. The integral light yield of segments of alpha tracks at known distances from the source, in the arbitrary digital units (ADU) of the CCD, is compared to the SRIM simulation [19] prediction for the visible energy loss in that segment. The segment length is chosen such that the SRIM prediction for the energy loss in each segment is 100–1000 keV, depending on the location and size of the segment along the alpha track. This procedure is done in the

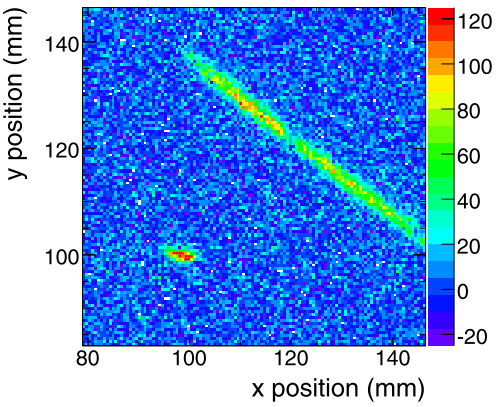

Fig. 2. A sub-region of a background-subtracted event from the top camera containing a segment of an alpha track (long) and a candidate nuclear recoil (short); intensity is in units of ADU, indicated by color (white pixels have < -20 ADU). Both tracks exhibit an asymmetry of energy loss along the axis of the track, consistent with the Bragg curve.

region of the alpha track where the alpha energy is above 1 MeV (before the Bragg peak). According to SRIM, at these energies, the alpha energy loss is $> 97\%$ electronic and so we are not sensitive to assumptions about the nuclear quenching in this calibration. This procedure gives the energy calibration of 9.5 ± 0.5 and 12.9 ± 0.7 ADU/keV respectively for the top and bottom cameras. After accounting for the different conversion gain and read noise for each camera, the signal-to-noise is approximately the same between the two. The uncertainty on the calibration is estimated by varying the size and location of the alpha segments relative to the start of the alpha track.

The system gain (ADU/keV) may vary with position and in time. The gain non-uniformity across the field of view due to local variations of the amplification is measured with a 14 μCi ^{57}Co source, which provides uniform illumination of the field-of-view from scattered 122 keV photons. The track-finding algorithm does not identify distinct tracks in the ^{57}Co data, largely because these fail the requirement of having at least five contiguous pixels above threshold (described further below). This is consistent with the predicted low ionization density of electron-like tracks (see, for example Fig. 16 in [5]). Rather, these events may have a few pixels above background in the entire field of view. To obtain high statistics, each gain non-uniformity measurement is integrated over 10,000 seconds; from calculation, the intensity and position of the source are such that the area imaged by each CCD pixel is covered by at least one electron recoil per second. The measurement yields a 10% variation of the total system gain, which is included as a position-dependent correction in the gain systematic study in Section 2.2. The stability of the gain vs. time was measured to be 1% over 24 hours using an ^{241}Am alpha source. To maintain 1% gain uniformity, the chamber is evacuated to 10 mTorr and refilled with CF_4 every 24 hours.

In the track reconstruction, raw CCD images are first background subtracted using an average of 100 dark frames (taken with the shutter closed) to remove spatial non-uniformities in the CCD dark rate. Dark frames are collected every 1000 exposures; $\geqslant 10\sigma$ lone outlier pixels are replaced with the mean of the 8 neighboring pixels before averaging. After dark frame subtraction, the same lone pixel cleaning procedure is applied to each image. For events which are not classified as sparks, any residual mean pixel count is removed by subtracting the mean pixel intensity of the image. The track finding algorithm bins the CCD images in software to 8×8 pixels. Groups of five contiguous bins with at least 3.7σ counts per bin are identified as clusters; 3.7 is chosen to optimize the energy reconstruction resolution. Clusters which lie within three bins of each other are combined, to account for the resistive separators segmenting tracks. Example tracks are shown in Fig. 2. Reconstructed quantities are determined from the original pixels (4×4 binned in readout) in each cluster.

The visible track energy is determined by the integral of the counts in a track, divided by the energy calibration constant (ADU/keV). To convert visible energy to nuclear recoil energy (shown in Figs. 3–5) we use the CF_4 quenching factor calculated in [20], and the SRIM prediction of nuclear and electronic energy loss for fluorine. The projected range of a track on the image plane is calculated as the distance between the maximally separated pixels in the track with yield $> 3.7\sigma$ above the image mean, multiplied by the length calibration constant (μm/pixel). The track angle in the amplification plane (ϕ) is determined by finding the major axis angle of an ellipse with the same second moment as the pixels in the cluster. The sense of the direction is estimated from the skewness of the track light yield.

The recoil energy and angle reconstruction resolution are 15% and 40° at 50 keV visible energy (80 keV nuclear recoil energy). The energy resolution is measured with alpha calibration data (shown in [18, Fig. 2]), and the energy resolution in Monte Carlo is validated by comparison with the measured energy resolution in alpha track segments. From nuclear recoil Monte Carlo, the energy resolution varies with energy as $(\sigma_E/E_{vis})^2 = a^2 + (b/\sqrt{E_{vis}})^2 + (c/E_{vis})^2$ where $a = 0.051$, $b = 3.8 \times 10^{-3}$, and $c = 6.1$, for events passing the nuclear recoil selection cuts described in the following section. The angular resolution is estimated with a Monte Carlo simulation of fluorine recoils from the ^{252}Cf calibration source. The simulation is based on measured detector characteristics [14,18]; the ^{252}Cf-F Monte Carlo is compared with data in Fig. 3. From Monte Carlo, the direction reconstruction resolution varies with energy as $(\sigma_\phi/E_{vis}) = a\exp(-E_{vis}/b)$ where $a = 6.1$ and $b = 24.3$, for events passing the nuclear recoil selection cuts described in the following section. More detail on directionality studies with this detector technology can be found in [17].

2.2. Surface run results

A major goal of the surface run was to identify detector backgrounds prior to underground operations. We found two broad categories: events which produce ionization outside the TPC drift volume, and events which occur inside it. A summary is given in Table 1.

Background events producing ionization outside the fiducial volume are mostly interactions of cosmic rays or radioactivity in the CCD chip, which is a well documented phenomenon [21]. These may be removed in the future by requiring coincidence of CCD and charge or PMT readout; in this CCD-only analysis, we reject these events in software. Such tracks typically have a few bins with very high yields. We identify these events by the large ADU and RMS of the pixels comprising the track. Another type of outside event is associated with sparks in the amplification region. Sparks are identified by having an image mean which differs by $> 1\%$ from the previous image. For comparson, images containing very bright alpha tracks differ in this metric by $< 0.01\%$. Sparks may induce residual bulk images (RBIs), which appear at the same spatial position for many subsequent images. RBIs are the result of the leakage of charge from the epitaxial/substrate interface of the CCD; these are a well-known background in front-illuminated CCDs associated with interactions of > 600 nm photons in the chip [21,22]. We identify these events by their coincident positions.

Background events producing ionization inside the fiducial volume come primarily from alphas and neutrons. Alpha particles

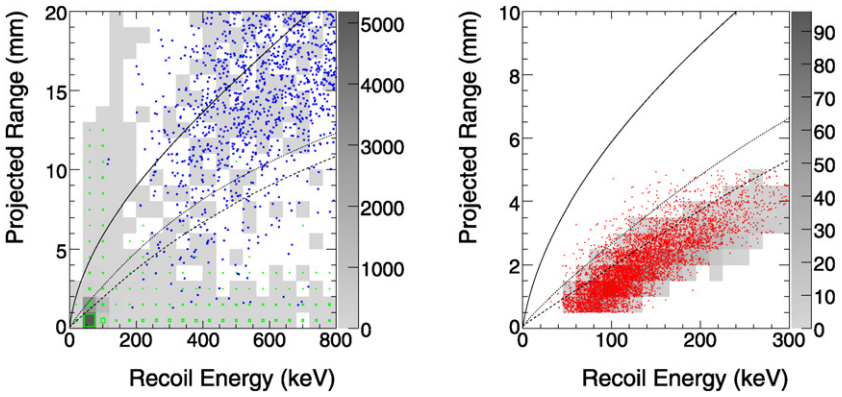

Fig. 3. Reconstructed projected range (mm) vs. reconstructed energy (keV). Left: the background populations; RBIs (shaded squares), alphas (blue points), and CCD interactions (green open boxes). Right: ^{252}Cf calibration data (red points) compared with ^{252}Cf-F Monte Carlo (shaded squares) after nuclear recoil selection cuts. Lines are SRIM predictions for the maximum projected range vs. recoil energy for helium (solid), carbon (dotted), and fluorine (dashed) nuclei.

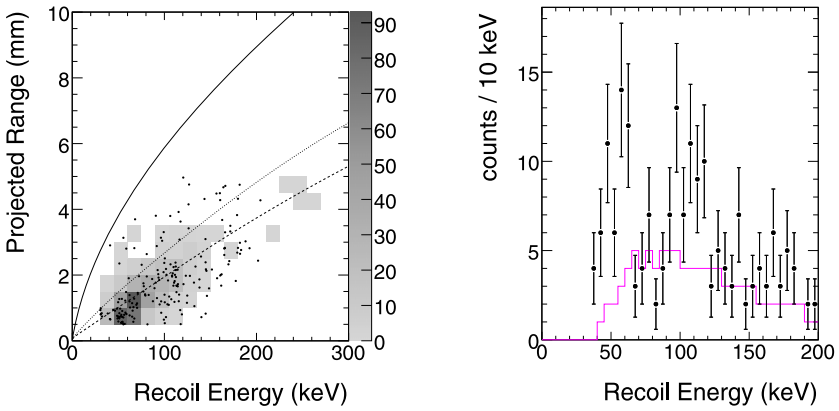

Fig. 4. Left: reconstructed projected range (mm) vs. reconstructed energy (keV) for WIMP-search data (black points) compared with 200 GeV/c^2 WIMP-F Monte Carlo (shaded squares) after nuclear recoil selection cuts. Lines are SRIM predictions for the maximum projected range vs. recoil energy for helium (solid), carbon (dotted), and fluorine (dashed) nuclei. Right: reconstructed energy (keV) for WIMP-search data passing nuclear recoil selection cuts (black points with statistical errors), and the predicted neutron-induced background (magenta line). (For interpretation of the references to colour in this figure legend, the reader is referred to the web version of this Letter.)

Table 1
Surface run event rates (Hz) after each background rejection cut, summed over the two cameras.

Event selection cut	Rate (Hz)
All tracks	0.43
Residual bulk images	0.15
CCD interactions	4.4×10^{-3}
Alpha candidates	8.2×10^{-5}
Nuclear recoil candidates in $80 < E_R < 200$ keV	5.0×10^{-5}

are emitted by radio-impurities in or on the materials of the detector; the majority are from the stainless steel drift cage. These are identified as CCD edge-crossing tracks. Another characteristic of alphas is their long range; we require nuclear recoils to have projected ranges < 5 mm. This range vs. energy discrimination is unique to tracking detectors. Fig. 3(left) shows events identified as alpha particles in comparison with the SRIM prediction for the maximum projected range vs. visible energy; tracks which are not parallel to the image plane have projected ranges less than this maximum. The ambient neutron flux comes from ^{238}U and ^{232}Th decays, and from cosmic ray spallation. Fig. 3(right) shows calibration ^{252}Cf neutron-induced recoils, which are indistinguishable from a dark matter signal on an event-by-event basis in range vs. energy; these tracks sample a range of angles relative to the amplification plane and are shown compared with the SRIM prediction for the maximum projected range vs. energy and to the detector simulation. There is no evidence for gamma-induced electron backgrounds [23]; the measured rejection is $> 10^6$.[1] The events remaining after all background cuts are shown in Fig. 4(left), compared to WIMP Monte Carlo.

We set a limit on the spin-dependent WIMP-proton interaction cross section using the method described in [16]. The signal efficiency is calculated from the WIMP Monte Carlo simulation. The analysis energy window, 80–200 keV, is chosen to maximize the integral above threshold of the product of efficiency and predicted WIMP-induced recoil spectrum (for $m_{WIMP} = 200$ GeV/c^2); this averaged efficiency is maximized at 70% at 80 keV threshold energy. There are 105 events after all cuts in $80 < E_{recoil} < 200$ keV, with 74 predicted neutron background events in this window based on the surface neutron spectrum measurement in [26] (Fig. 4(right)). We do not take into account the building around the detector, and so assign 100% uncertainty to the neutron background and report the limit assuming zero expected events. Using the Feldman–Cousins method [27], we set a 90% confidence level limit on the spin-dependent WIMP-proton cross section, shown in

[1] The study in [23] used an 8 μCi ^{137}Cs calibration source, positioned on the drift mesh inside the detector, for 1/3 day. No tracks were identified by the reconstruction algorithm; the rejection factor comes from comparing the observed with the expected number of 661 keV betas associated with the ^{137}Cs decay. From simulation, we find that betas do not satisfy the track-finding algorithm requirement of 5 contiguous pixels with signal-to-noise ratio above the 3.7σ threshold [5].

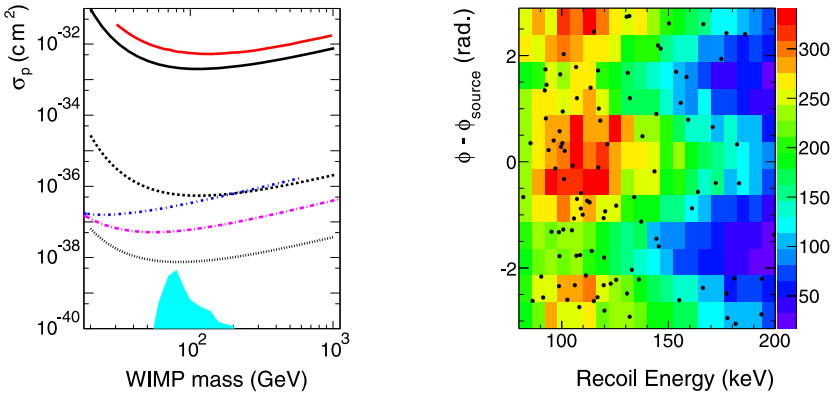

Fig. 5. Left: 90% confidence level limit on the spin-dependent WIMP-proton cross section vs. dark matter particle mass from DMTPC surface data (black solid line), compared with the NEWAGE [8] underground directional result (red solid line), and the two leading limits from conventional detectors, COUPP [24] (magenta dash-dotted line) and PICASSO [25] (blue dash-dotted line). The cyan shaded region shows MSSM parameter space [2]. The projected sensitivity for DMTPC at WIPP, with 1 year exposure (black dashed line), and a 1 m^3 detector at WIPP with 50 keV energy threshold (black dotted line), are also shown. Right: reconstructed angle relative to source ϕ–ϕ_{source} (radians) vs. recoil energy (keV) for data passing nuclear recoil selection cuts in the dark matter search energy range; WIMP search data (black points) is compared with ^{252}Cf data (color indicates number of events). For WIMP search data ϕ_{source} is the direction to Cygnus, for ^{252}Cf data ϕ_{source} is the direction to the source in the laboratory (which is effectively a point source).

Fig. 5(left). Following [16], we use the thin-shell spin-dependent form factor approximation, and the interaction factor $C^2_{Wp} = 0.46$ for Higgsino-proton coupling. The 90% C.L. cross section upper limit is 2.0×10^{-33} cm^2 at 115 GeV/c^2 WIMP mass. If we vary the gain non-uniformity by 100%, the limit is $< 2.3 \times 10^{-33}$ cm^2. If we include the estimated background of 74 events, the limit is $< 8.0 \times 10^{-34}$ cm^2.

We evaluate the probability that events passing the nuclear recoil selection cuts come from an isotropic background vs. anisotropic WIMP-induced recoil angle distribution. The Rayleigh statistic is a powerful tool to analyze the uniformity of a distribution of angles when looking for a preferred direction [28]. Using the Rayleigh statistic, we quantify the anisotropy in (ϕ–ϕ_{source}), which is the most sensitive variable to test for anisotropy in the case of two-dimensional readout [29]. (ϕ–ϕ_{source}) is the difference between the reconstructed ϕ and the projection of the expected dark matter direction at the time of each event onto the image plane. The (ϕ–ϕ_{source}) vs. E_R distribution after nuclear recoil selection cuts in is shown in Fig. 5(right). We find no statistically significant deviation from a uniform distribution; 36% of the time uniformly distributed data have a Rayleigh value higher than that of our candidate events. The reconstructed angle of the ^{252}Cf calibration data relative to its source is also shown in Fig. 5 (right). The ^{252}Cf calibration source is effectively a point source in the lab frame at $\phi_{source} = 0$. The Rayleigh test applied to the ^{252}Cf calibration data after the nuclear recoil selection cuts, in the same recoil energy range (80–200 keV), gives a probability of $< 1\%$ for a uniform distribution.

3. Conclusions

We present the first dark matter limit from DMTPC, $\sigma_{\chi-p} < 2.0 \times 10^{-33}$ cm^2 at 90% C.L., from a 35.7 g-day surface exposure of a 10 liter detector. The 10^4 rejection of backgrounds using range vs. energy properties of nuclear recoils, from Table 1, is an impressive demonstration of the low pressure directional time projection chamber concept. We find that the backgrounds in the analysis window of 80–200 keV are qualitatively consistent with the predicted neutron background. The 10-L detector described here began running underground at the Waste Isolation Pilot Plant outside Carlsbad, NM in October 2010. The depth of the WIPP site is 1.6 km water-equivalent. The gamma, muon, and radon background levels have been measured, and the neutron background has been estimated at this site [30]. Based on these, we project that underground operation will lower the expected neutron background to < 1 event/year. The projected zero background sensitivity of this detector at WIPP for a 1 year exposure is shown in Fig. 5(left). DMTPC has built a second-generation detector with radio-pure materials for operation at WIPP; this is expected to substantially reduce alpha backgrounds, and fiducial volume coverage by CCDs in coincidence with charge readout will eliminate CCD backgrounds. At the scale of a 1 m^3 detector (300 g target), which the collaboration is actively developing, this detector technology is competitive with the best current spin-dependent cross section limits from conventional dark matter detectors, also shown in Fig. 5(left).

Acknowledgements

We acknowledge support by the Advanced Detector Research Program of the US Department of Energy (contract number 6916448), as well as the Reed Award Program, the Ferry Fund, the Pappalardo Fellowship program, the MIT Kavli Institute for Astrophysics and Space Research, the MIT Bates Research and Engineering Center, and the Physics Department at the Massachusetts Institute of Technology. We would like to thank Mike Grossman for valuable technical assistance.

References

[1] D.N. Spergel, et al., WMAP Collaboration, Astrophys. J. Suppl. 170 (2007) 377, astro-ph/0603449.
[2] J.R. Ellis, A. Ferstl, K.A. Olive, Phys. Rev. D 63 (2001) 065016, hep-ph/0007113.
[3] D. Hooper, E. Baltz, Annu. Rev. Nucl. Part. Sci. 58 (2008) 293, arXiv:0802.0702 [hep-ph].
[4] R.J. Gaitskell, Annu. Rev. Nucl. Part. Sci. 54 (2004) 315.
[5] S. Ahlen, et al., Int. J. Mod. Phys. 25 (2010) 1, arXiv:0911.0323 [astro-ph].
[6] K.N. Buckland, M.J. Lehner, G.E. Masek, M. Mojaver, Phys. Rev. Lett. 73 (1994) 1067.
[7] G.J. Alner, et al., Nucl. Instrum. Meth. A 555 (2005) 173.
[8] K. Miuchi, et al., NEWAGE Collaboration, Phys. Lett. B 686 (2010) 11, arXiv:1002.1794v1.
[9] D. Dujmic, et al., Nucl. Instrum. Meth. A 584 (2008) 327, arXiv:0708.2370.
[10] D. Santos, O. Guillaudin, T. Lamy, F. Mayet, E. Moulin, J. Phys. Conf. Ser. 65 (2007) 012012, astro-ph/0703310.
[11] T. Naka, et al., Nucl. Instrum. Meth. A 581 (2007) 761.
[12] D.N. Spergel, Phys. Rev. D 37 (1988) 1353.
[13] A.M. Green, B. Morgan, Astropart. Phys. 27 (2007) 142, astro-ph/0609115.
[14] A. Kaboth, et al., Nucl. Instrum. Meth. A 592 (2008) 63, arXiv:0803.2195 [physics.ins-det].

[15] G. Jungman, M. Kamionkowski, K. Griest, Phys. Rept. 267 (1996) 195, hep-ph/9506380.
[16] J.D. Lewin, P.F. Smith, Astropart. Phys. 6 (1996) 87.
[17] D. Dujmic, et al., Astropart. Phys. 30 (2008) 58, arXiv:0804.4827 [astro-ph].
[18] T. Caldwell, et al., arXiv:0905.2549 [physics.ins-det], 2009.
[19] J.F. Ziegler, J.P. Biersack, U. Littmark, The Stopping and Range of Ions in Solids, Pergamon Press, New York, 1985, http://www.srim.org.
[20] A. Hitachi, Rad. Phys. Chem. 77 (2008) 1311, arXiv:0804.1191.
[21] J.R. Janesick, Scientific Charge-Coupled Devices, SPIE Press Monograph PM83, 2001.
[22] A. Rest, et al., Rev. Sci. Instrum. 73 (5) (2002) 2028.
[23] D. Dujmic, et al., J. Phys. Conf. Ser. 120 (2008) 042030, arXiv:0801.2687 [astro-ph].
[24] E. Behnke, et al., arXiv:1008.3518, 2010.
[25] S. Archambault, et al., PICASSO Collaboration, Phys. Lett. B 682 (2009) 185, arXiv:0907.0307.
[26] T. Nakamura, T. Nunomiya, S. Abe, K. Terunuma, H. Suzuki, J. Nucl. Sci. Technol. 42 (10) (2005) 843.
[27] G.J. Feldman, R.D. Cousins, Phys. Rev. D 57 (1998) 3873, physics/9711021.
[28] K. Mardia, P. Jupp, Directional Statistics, Wiley, New York, 2000.
[29] B. Morgan, A.M. Green, Phys. Rev. D 72 (2005) 123501, astro-ph/0508134.
[30] E.-I. Esch, Ph.D. thesis, 2001, lA-UR-01-3974.